Aerodynamic behavior of an airfoil with morphing trailing edge for wind turbine applications

2014 J. Phys.: Conf. Ser. 524 012018

(http://iopscience.iop.org/1742-6596/524/1/012018)

Aerodynamic behavior of an airfoil with morphing trailing edge for wind turbine applications

T Wolff[1], B Ernst and J R Seume

ForWind - Center for Wind Energy Research, Leibniz Universitaet Hannover,
Institute of Turbomachinery and Fluid Dynamics - TFD,
Appelstr. 9, 30167 Hanover, Germany

E-mail: wolff@tfd.uni-hannover.de, seume@tfd.uni-hannover.de

Abstract. The length of wind turbine rotor blades has been increased during the last decades. Higher stresses arise especially at the blade root because of the longer lever arm. One way to reduce unsteady blade-root stresses caused by turbulence, gusts, or wind shear is to actively control the lift in the blade tip region. One promising method involves airfoils with morphing trailing edges to control the lift and consequently the loads acting on the blade. In the present study, the steady and unsteady behavior of an airfoil with a morphing trailing edge is investigated. Two-dimensional Reynolds-Averaged Navier-Stokes (RANS) simulations are performed for a typical thin wind turbine airfoil with a morphing trailing edge. Steady-state simulations are used to design optimal geometry, size, and deflection angles of the morphing trailing edge. The resulting steady aerodynamic coefficients are then analyzed at different angles of attack in order to determine the effectiveness of the morphing trailing edge. In order to investigate the unsteady aerodynamic behavior of the optimal morphing trailing edge, time-resolved RANS-simulations are performed using a deformable grid. In order to analyze the phase shift between the variable trailing edge deflection and the dynamic lift coefficient, the trailing edge is deflected at four different reduced frequencies for each different angle of attack. As expected, a phase shift between the deflection and the lift occurs. While deflecting the trailing edge at angles of attack near stall, additionally an overshoot above and beyond the steady lift coefficient is observed and evaluated.

1. Introduction

During the last decades, the length of wind turbine rotor blades increased in response to the demand for higher power generation per wind turbine, see Kaldellis and Zafirakis [1]. Complex flow environments with wind shear, turbulences, and gusty wind conditions cause high unsteady loading on increasingly long and slender rotor blades, see Kelley et al. [2]. Due to the longer lever arm which accompanies longer blades higher stresses arise, particularly at the blade root. One way to reduce these blade-root stresses is to reduce the forces acting near the blade tip region, achieved by reducing the lift coefficient in this region. Airfoils with morphing trailing edges applied to the outer blade region of the wind turbine are a promising method to actively control the lift coefficient and consequently the loads acting on the blade, see Barlas and van Kuik [3].

[1] Address all correspondence to this author.

The application of trailing edge flaps and deformable trailing edges on wind turbine blades is inspired by existing applications on aircraft wings and helicopter blades, but with different control objectives. In general, there are two approaches for the application of deformable trailing edges on wind turbine blades. On the one hand, the change in lift due to the trailing edge deflection can be used for power control, on the other hand, the loads acting on the wind turbine can be reduced using the deformable trailing edge by adjusting the lift depending on the transient wind conditions. An important requirement is the parking capability by solely using deformable trailing edges for power control. Studies of trailing edge flaps and deformable trailing edges applied to wind turbine blades have already been carried out, including numerical and experimental investigations. The wind tunnel tests carried out by Pechlivanoglou et al. [4] showed that the lift of a wind turbine airfoil can be directly controlled by an adaptive trailing edge geometry. Pechlivanoglou et al. [4] indicate, however, that it is not always possible to reach a lift-to-drag-ratio equal or close to zero, which is necessary for a shut down or at wind conditions in which the rotor is just idling. Therefore, the deformable trailing edge cannot be used as the sole control system. Similar conclusions have been drawn by Bak et al. [5]. The wind tunnel tests by Bak et al. [5] performed with a Riso-B1-18 airfoil have shown that deflecting the trailing edge can considerably influence lift and drag. Investigations made on the same profile than the one used in the present work (DU08-W-180-6.5) but equipped with a rigid flap were performed by Ortega Gomez et al. [6]. The authors calculated profile polars for different deflection angles of the flap using the panel method solver XFoil and evaluated if the flap is sufficient to replace the pitch control system. For high wind speed fluctuations, it was shown that the change in lift and drag - due to flap actuations - is not high enough for the power and load control of the wind turbine. Troldborg [7] carried out extensive simulations in order to derive an optimal trailing edge geometry using the 2D incompressible RANS solver EllipSys2D. In addition to the parameter study based on steady-state simulations, transient flow phenomena are investigated by means of simulations with harmonic pitch oscillations and/or oscillatory motions of the deformable trailing edge. In conclusion, Troldborg's work suggests that a curved trailing edge with a relative length between 5% and 10% of the chord length is a good compromise between the ability to control the lift and the actuator power needed to deflect the trailing edge.

In order to reduce unsteady loads of wind turbine rotor blades caused by turbulent inflow conditions and gusts, the main focus of the present study is to design an optimal deformable trailing edge geometry for the DU08-W-180-6.5 airfoil and to analyze the effect of the actively deformed trailing edge on the flow characteristics. First, steady-state computations are carried out to evaluate the trailing edge's effectiveness in terms of the coefficients of lift, of drag, and of the flap-hinge moment. Second, unsteady phenomena, i.e. dynamic stall and the phase shift between trailing edge deflection and lift coefficient, are investigated by time-resolved simulations of the actively deflected trailing edge using a deformable grid approach.

2. Airfoil Geometry

In the present study the DU08-W-180-6.5 airfoil designed at the TU Delft [8] is investigated. This is a typical thin airfoil which can be used in the outer part of modern wind turbine blades. Deformable trailing edges are particularly desirable in this region because they have a large impact on the blade root bending moments. The reference DU08-W-180-6.5 airfoil, which is shown in figure 1a, has a thickness-to-chord ratio of $t/c = 0.18$ and has a blunt trailing edge of height $t_{\mathrm{te}} = 6.5$ mm. In the present study, all simulations are conducted with a normalized chord length of $c = 1$ m. Several geometries of the deformable trailing edge have been designed for the parameter study in section 4. The beginning of the trailing edge's morphing, or the relative chord length of the morphing trailing edge, was varied between $c_{\mathrm{mte}} = c_{\mathrm{te}}/c = 0.05$ (c_{te} describes the chordwise position, starting from the trailing edge, at which the morphing of the trailing edge begins) and $c_{\mathrm{mte}} = 0.3$ in steps of $\Delta c_{\mathrm{mte}} = 0.05$. The deflection angles chosen

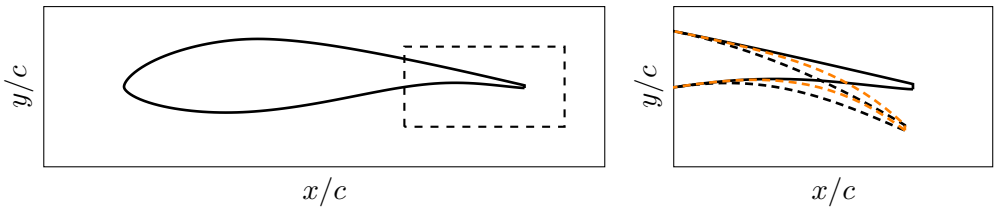

(a) Reference airfoil

(b) Reference and deflected trailing edge

Figure 1. Geometry of the DU08-W-180-6.5 airfoil with undeflected trailing edge (——) and with $\beta = 10$ deg deflected trailing edge ($c_{\mathrm{mte}} = 0.3$), gently (- - - -) and strongly (- - - -) curved

ranged from $\beta = -10$ deg to $\beta = 10$ deg in steps of $\Delta\beta = 5$ deg. A positive deflection angle describes a deflection to the pressure side and a negative deflection angle describes a deflection to the suction side. Two different shapes of the trailing edge deformation have been used, one with a gently (quadratic function) and the other with a strongly (cubic function) curved trailing edge (see figure 1b). A rigid flap (linear function) is not considered, because it can be assumed that the performance of a rigid flap is worse than a curved deformation of the trailing edge (see Troldborg [7]).

3. Numerical Model

3.1. Flow Solver

The aerodynamic design code FLOWer, developed by the German Aerospace Center (DLR), German universities, and Airbus Germany [9], is used for the numerical simulations. FLOWer solves the two- and three-dimensional Reynolds-averaged Navier-Stokes equations using structured multi-block meshes and a finite-volume approach. The convective fluxes are discretized by a central discretization scheme according to Jameson [10]. The closure problem of the Reynolds equations is solved by substituting the Reynolds-stress tensor by a one-equation Spalart-Allmaras model with Edwards modification [11]. This turbulence model was chosen because of its good convergence even at stall. All boundary layers are assumed to be fully turbulent.

All steady-state computations are solved with an explicit Runge-Kutta time integration scheme. Implicit residual smoothing and a multigrid approach are used to accelerate convergence. Convergence of the simulations is assumed to be reached when the maximum residual of the density is less than 10^{-3} and the maximum change in lift and drag coefficient from one iteration to the following is at or below 10^{-4}.

The time-resolved simulations use a second-order accurate implicit dual-time stepping scheme. A deformable grid approach, which uses linear interpolation to interpolate between given meshes, is used to simulate the morphing trailing edge. A non-dimensional time step of $t^* = 0.5$ is used.

3.2. Mesh

The computational region includes the two-dimensional airfoil surrounded by an O-grid (see figure 2) with a radius of $50{\cdot}c$ to ensure that there are no reflecting influences from the boundaries. There are 336 grid points in the circumferential direction and 96 in the radial direction. The first cell distance normal to the airfoil suction and pressure sided surface was defined small enough so that the dimensionless wall distance equals $y^+ \approx 1$. The boundary layer region is resolved with 48 cell layers in the direction normal to the airfoil surface. The whole mesh consists of approximately 40.000 nodes. The boundary layer on the blunt part of the trailing edge was not

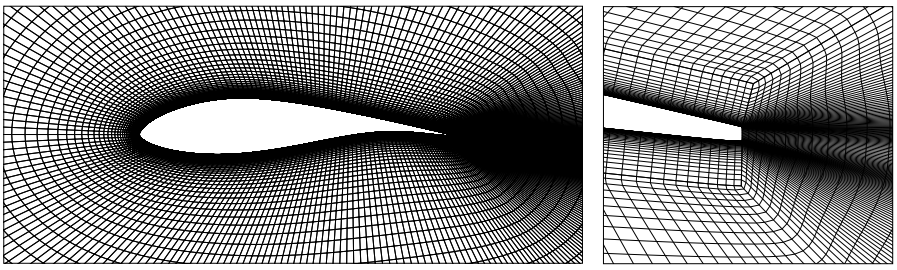

(a) Overview (b) Trailing edge

Figure 2. Computational grid around the airfoil and detailed view on the trailing edge grid with undeflected trailing edge

resolved. Resolving the boundary layer in this region would have led to meshing problems due to the use of an O-grid. It is assumed that the relative comparisons in this work are not significantly influenced by following this procedure. A grid with C-H-topology and resolved boundary layer was generated to quantify the difference between the resolved and not resolved boundary layer. This grid topology was not stable at most of the configurations, so that a comparison could not have been performed.

A grid convergence study has been conducted in accordance with the ASME V & V 20 Committee [12] to determine the discretization error. For this purpose, a mesh with half of the distance between nodes and a mesh with quarter of the distance between nodes in each dimension compared to the reference mesh have been generated. The lift coefficient c_l and the drag coefficient c_d, as plotted in figure 3 are chosen as the values for the evaluation of convergence f. The grid convergence index (GCI) is defined as

$$GCI = \frac{F_s \cdot \left| \frac{f_\mathrm{Fine} - f_\mathrm{Coarse}}{f_\mathrm{Coarse}} \right|}{r^p - 1}. \tag{1}$$

F_s describes a safety factor which is $F_s = 1.25$, r is the grid refinement, defined as $r = (N_\mathrm{Fine}/N_\mathrm{Coarse})^{(1/D)}$ with the number of grid cells N and the number of refinement dimensions D, and p is the calculation order, which was conservatively set to $p = 1$. The results show a GCI for the used grid of $GCI_{c_\mathrm{l}} = 1.1\%$ concerning the lift coefficient c_l and $GCI_{c_\mathrm{d}} = 21.6\%$ concerning the drag coefficient c_d. The relatively large GCI_{c_d} can be explained by the conservatively chosen grid order $p = 1$. The value for the GCI concerning c_d is $GCI_{c_\mathrm{d}} = 9.1\%$ if the GCI is determined with the calculated $p = 1.75$.

3.3. Boundary Conditions

The airfoil surface is defined as a no-slip wall. The boundary of the computational region is set as a farfield boundary. The Reynolds number

$$Re = \frac{U \cdot c \cdot \rho}{\mu} \tag{2}$$

(U describes the magnitude of the flow velocity, ρ the density of the flow and μ the dynamic viscosity) is chosen as $Re = 5 \cdot 10^6$ at the design tip speed. The Mach number

$$Ma = \frac{U}{a} \tag{3}$$

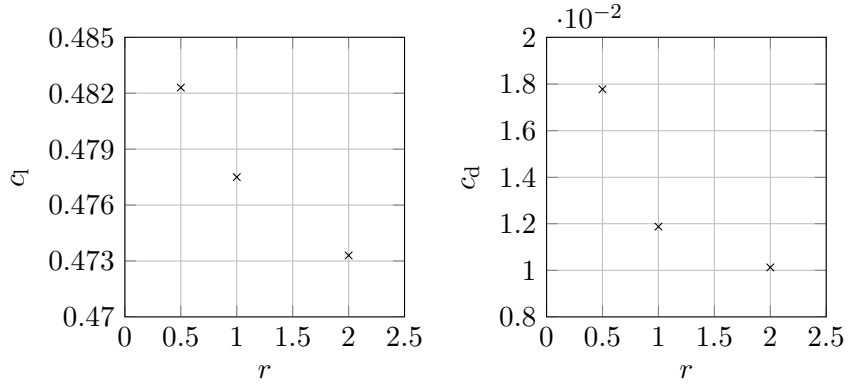

(a) c_l (b) c_d

Figure 3. Lift coefficient c_l and drag coefficient c_d plotted against the grid refinement r

is chosen as $Ma = 0.265$. The turbulence intensity is set to 5%. The angle of attack is varied between $\alpha = -12$ deg and $\alpha = 12$ deg. Simulations with six different angles of attack in the range between $\alpha = 0$ deg and $\alpha = 10$ deg are performed for the time-resolved investigations with actively deformed trailing edges. Four different reduced frequencies k are examined for each angle of attack in order to describe the trailing edge motion. The reduced frequency k is defined as

$$k = \frac{\omega \cdot c}{2 \cdot U}, \tag{4}$$

with ω being the frequency of the trailing edge motion. According to Hansen [13], flutter can occur in wind turbines at a reduced frequency $k \ll 1$. Thus, values between $0.1 < k < 0.4$ have been chosen in the similar range as in Troldborg [7]. The higher the reduced frequency, the faster is the trailing edge motion and the better is the ability of the trailing edge motion to react on unsteady flow conditions. However, only one single trailing edge motion is simulated described by half a period of a cosine-curve, starting from $\beta = 0$ deg and reaching its amplitude at $\beta = 10$ deg.

4. Parameter Study

A parameter study of the gently curved trailing edge has been carried out and is described in this section. First, the effects of the relative trailing edge length c_mte and the deflection angle β on the lift and drag coefficients are discussed. Second, the effectiveness of the flap is evaluated by considering the sensitivity of the coefficients of lift and of the flap-hinge moment with respect to various parameters. Finally, an optimal geometry based on the results of the parameter study is recommended.

4.1. Lift and Drag Coefficients

The lift coefficient c_l and the lift-to-drag ratio $c_\mathrm{l}/c_\mathrm{d}$ are plotted against the angle of attack α for different trailing edge configurations in figure 4. The flow deviation increases if the deflection angle β is positive and decreases if the deflection angle β is negative. This leads to higher (positive deflection) or lower (negative deflection) lift coefficients (see figure 4a). An increasing size of the deflected trailing edge c_mte amplifies these effects.

The additional flow deviation due to the deflected trailing edge is smaller at angles of attack close to the stall angle. This results in a decreasing sensitivity of the lift coefficient to changes in angle of attack at higher angles of attack and different positive deflection angles β (see figure 4a). The same effect appears for negative angles of attack and negative deflection angles.

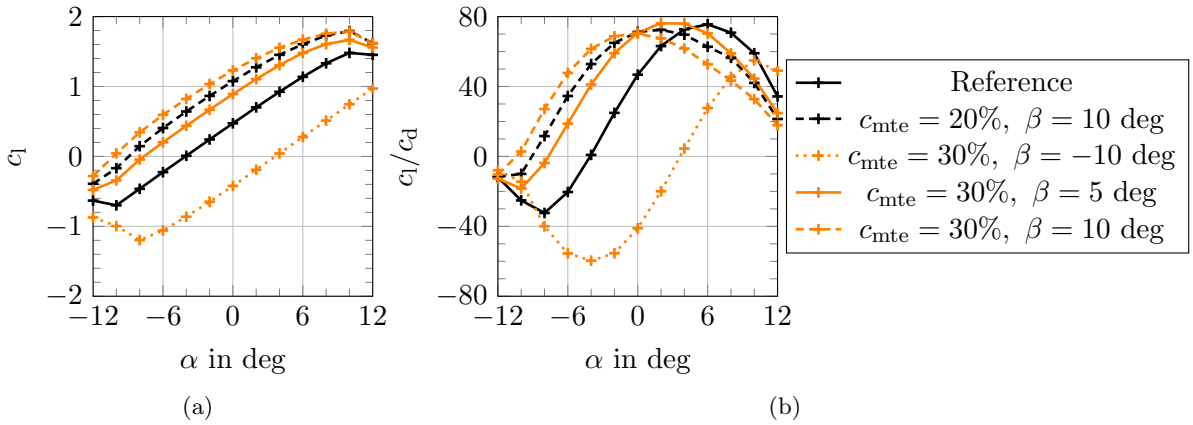

Figure 4. Lift coefficient c_l and lift-to-drag ratio $c_\mathrm{l}/c_\mathrm{d}$ plotted against the angle of attack α for a variation of deflected trailing edges

Another consequence of the changed flow deviation due to the trailing edge deflection is the changed stall behavior. For positive angles of attack, an increased flow deviation as caused by a positively deflected trailing edge leads to instant flow separation at small angles of attack. Negative deflection angles β of the trailing edge and an accompanied decreased flow deviation delay the flow separation at positive angles of attack, and vice versa positive deflection angles β of the trailing edge delay the flow separation at negative angles of attack. This is shown in figure 4a, where stall occurs on the reference airfoil at angles of attack $\alpha \gtrsim 10$ deg and $\alpha \lesssim -10$ deg, respectively. By deflecting 30% of the chord length by $\beta = -10$ deg (see figure 4a, ···+···) leads to stall at angles of attack $\alpha \lesssim -8$ deg and $\alpha > 12$ deg.

The effect of the deflected trailing edge on the lift-to-drag ratio is shown in figure 4b. The increased lift caused by positive trailing edge deflections increases the lift-to-drag ratio compared to the reference airfoil at angles of attack between $\alpha = -12$ deg and approximately $\alpha \approx 3$ deg. The increased drag which accompanies a positively deflected trailing edge (larger cross section perpendicular to the flow direction) at positive angles of attack causes a decreasing lift-to-drag ratio at angles of attack $\alpha \gtrsim 3$ deg.

Using a different deflected shape of the trailing edge, e.g. a strongly curved trailing edge (see figure 1b) does not change the lift and drag coefficients significantly compared to the gently curved trailing edge. The main differences are a lower maximum lift-to-drag ratio of approximately 7% and an increase of the flap-hinge moment coefficient (see equation 5) by approximately 30% compared to the gently curved trailing edge ($c_\mathrm{mte} = 20\%,\ \beta = 10$ deg). Given its lower performance, the strongly curved trailing edge is not further investigated in the present study.

4.2. Flap Effectiveness Evaluation

When evaluating the effectiveness of a deformable trailing edge, several aspects have to be considered. Most importantly, the deflected trailing edge must generate the desired amount of additional or reduced lift to actively control the loads. An additional requirement that has to be fulfilled is a low drag and a high lift-to-drag ratio. The third aspect is that a low force is needed to deform the trailing edge so that the efficiency of the deformable trailing edge is as high as possible. In theory an optimal geometry could be found for every angle of attack, however this is not possible. Instead the angle of attack with the highest lift-to-drag-ratio of the reference airfoil ($\alpha = 6$ deg, see figure 4b) was used to determine an optimal geometry. This angle of attack is normally used as the control value for the pitch regulation and therefore it is the most

common operating condition.

In the present investigation, only aerodynamic and no structural aspects are considered during the evaluation of the force needed to deform the trailing edge. For that reason, the force needed is represented by the flap-hinge moment coefficient c_{fhm}, which is the integral of the product of the pressure coefficient c_{p} and the distance between the actual position x and the hinge point c_{te}:

$$c_{\mathrm{fhm}} = \int_{x=c-c_{\mathrm{te}}}^{x=c} c_{\mathrm{p}} \cdot \frac{x-(c-c_{\mathrm{te}})}{c_{\mathrm{te}}}\,\mathrm{d}x. \tag{5}$$

The flap-hinge moment can be interpreted as the aerodynamic force acting on the trailing edge. In addition, stall should be avoided when the trailing edge is deflected. Therefore, a safety margin between the actual flow conditions and stall must be preserved.

The discussion in section 4.1 shows that the deformed trailing edge changes the lift sufficiently while achieving a high lift-to-drag ratio. The flap effectiveness parameter defined by Troldborg [7]:

$$\eta_{\mathrm{flap}} = \frac{(\partial c_{\mathrm{l}}/\partial\beta)}{(\partial c_{\mathrm{l}}/\partial\alpha)} \tag{6}$$

describes the sensitivity of the lift coefficient to changes of the deflection angle, normalized by the change of the lift coefficient by changing the angle of attack. In figure 5a it is shown that the flap effectiveness parameter η_{flap} increases with an increasing length of the morphing trailing edge. Therefore, it is not possible to identify an optimal geometry of the morphing trailing edge solely based on this parameter.

In two ways, a parameter can be derived, which describes the lift generated by deflecting the trailing edge in relation to the aerodynamic force acting on the trailing edge. The first way relates the sensitivity of lift to deflection angle to the sensitivity of flap-hinge moment to deflection angle:

$$\eta_{\beta} = \frac{(\partial c_{\mathrm{l}}/\partial\beta)_{c_{\mathrm{mte}}=\mathrm{const.}}}{(\partial c_{\mathrm{fhm}}/\partial\beta)_{c_{\mathrm{mte}}=\mathrm{const.}}}. \tag{7}$$

The second way also describes the sensitivity of lift, but to the relative chord length of the deflected trailing edge:

$$\eta_{c_{mte}} = \frac{(\partial c_{\mathrm{l}}/\partial c_{\mathrm{mte}})_{\beta=\mathrm{const.}}}{(\partial c_{\mathrm{fhm}}/\partial c_{\mathrm{mte}})_{\beta=\mathrm{const.}}}. \tag{8}$$

The partial derivatives are calculated using the forward differencing scheme. This means that e.g. $\eta_{\beta}(\beta = 0 \text{ to } 5 \text{ deg})$ is calculated with the coefficients at $\beta = 0$ deg and $\beta = 5$ deg. This is also the reason why the values for $\eta_{c_{mte}}$ are plotted between two values of c_{mte} (see figure 5b). High values of this parameter indicate a high gain in lift per aerodynamic force acting on the trailing edge.

The characteristic change of the pressure distribution on the airfoil's surface is different at different relative chord lengths of the deformable trailing edge ($\beta = 10$ deg). The decrease of the pressure coefficient on the suction side of the airfoil in the first 40% of the chord is higher from $c_{\mathrm{mte}} = 10\%$ to $c_{\mathrm{mte}} = 20\%$ than from $c_{\mathrm{mte}} = 20\%$ to $c_{\mathrm{mte}} = 30\%$ (see figure 6, ①). The increase of the lift coefficient is the same for both cases. As a consequence, the lower decrease of the pressure coefficient near the leading edge in the latter case is assumed to be compensated with a higher increase of the pressure coefficient's difference near the trailing edge (compared to the former case). Hence, the change of the flap hinge moment coefficient becomes larger from $c_{\mathrm{mte}} = 20\%$ to $c_{\mathrm{mte}} = 30\%$. This leads to a lower flap effectiveness parameter $\eta_{c_{\mathrm{mte}}}$ at higher c_{mte} and a maximum of $\eta_{c_{\mathrm{mte}}}$ between $c_{\mathrm{mte}} = 15\%$ and $c_{\mathrm{mte}} = 20\%$ (see figure 5b). As a result, the increase of the force acting against the trailing edge motion becomes larger than the increase of lift at longer relative chord lengths than $c_{\mathrm{mte}} = 20\%$. Thus, using a length of the deformable trailing edge longer than $c_{\mathrm{mte}} = 20\%$ becomes less effective.

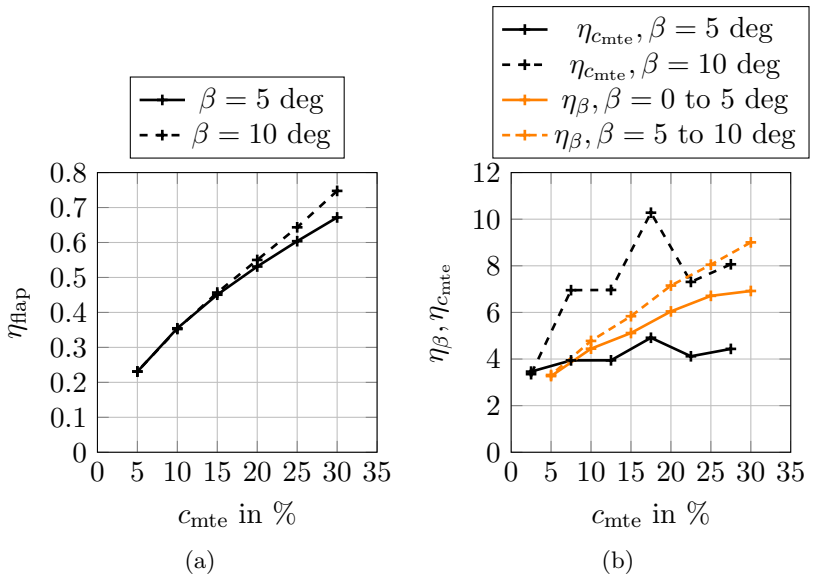

Figure 5. Effectiveness of the deflected trailing edge η_{flap}, η_β, and $\eta_{c_{\text{mte}}}$ plotted against the relative chord length of the trailing edge c_{mte} for a variation of deflected trailing edges at $\alpha = 6$ deg

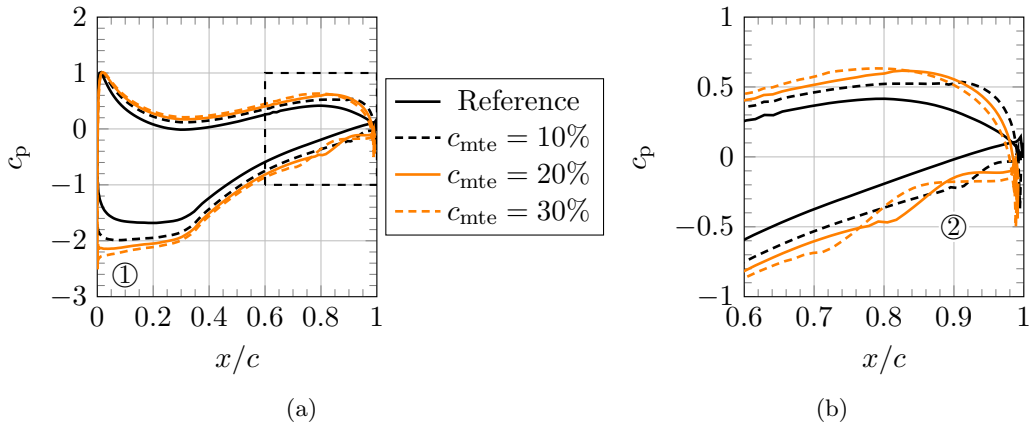

Figure 6. Pressure coefficient c_{p} plotted against the chord length for different relative chord lengths of the trailing edge at $\alpha = 6$ deg and $\beta = 10$ deg

Changing the deflection angle β does not have a significant impact on the characteristic change of the pressure distribution. This leads to a similar increase of c_{l} and c_{fhm} for larger deflection angles. Hence, η_β increases nearly monotonically with the length of the deflected trailing edge (see figure 5b).

Flow separation occurs at large trailing edge deflections if the flow is no longer able to follow the airfoil's surface. The region with separated flow increases with increasing length of the morphing trailing edge. This is shown in the detailed view of the pressure coefficient near the trailing edge in figure 6b. The flow separation can be identified by the increase of the pressure coefficient followed by a plateau with a nearly constant pressure coefficient (②).

4.3. Optimal Geometry

Different aspects have to be considered to evaluate the optimal geometry of the morphing trailing edge. The change of lift should be maximized while simultaneously minimizing the aerodynamic force acting on the trailing edge. Additionally, the stall behavior of the airfoil, which is highly dependent on the angle of attack, must not be modified. The results of the parameter study show that the lift as well as the force acting against the trailing edge motion increase with increasing deflection angle and length of the morphing trailing edge. For that reason, the ratio of the change in gained lift and aerodynamic force acting on the flap has to be taken into account to find a preferable compromise.

Even if there is no generally optimal geometry, the flap effectiveness parameter $\eta_{c_{\mathrm{mte}}}$ shows a maximum value at a length of the morphing trailing edge between $c_{\mathrm{mte}} = 15\%$ and $c_{\mathrm{mte}} = 20\%$. A shorter or longer morphing trailing edge decreases the flap effectiveness. The stall behavior of the airfoil is not changed significantly by using a length of the morphing trailing edge of $c_{\mathrm{mte}} = 20\%$. As a result, a relative chord length of $c_{\mathrm{mte}} = 20\%$ is used in the following time-resolved calculations. At larger deflection angles the flap effectiveness parameter η_β permanently increases with the relative chord length c_{mte} to an asymptotic maximum so that an optimal value for the deflection angle cannot be found by taking two different deflection angles β into account.

5. Unsteady Behavior of the Actively Deformed Trailing Edge

The results of the time-resolved simulations with the trailing edge motion using a deformable grid approach are described in this section. The dynamic change of the lift coefficient, the phase shift between lift coefficient and trailing edge motion as well as the overshoot of the lift coefficient are analyzed.

Shown in figure 7 are detailed views on the dynamic change of the lift coefficient zoomed in the region of the static lift coefficient during and after the trailing edge's motion for two different angles of attack. The time when the trailing edge reaches its maximum deflection ($\hat{\beta} = 10$ deg) and the motion is stopped is marked by •. $\Delta c_{\mathrm{l,Rel}}$ describes the ratio of the difference between the actual c_{l} and the static value of the lift coefficient at $\beta = 0$ deg to the difference between the static value of the lift coefficient at $\beta = 10$ deg and at $\beta = 0$ deg:

$$\Delta c_{\mathrm{l,Rel}} = \frac{c_{\mathrm{l}} - c_{\mathrm{l,static}}(\beta = 0 \text{ deg})}{c_{\mathrm{l,static}}(\beta = 10 \text{ deg}) - c_{\mathrm{l,static}}(\beta = 0 \text{ deg})}. \tag{9}$$

For an angle of attack of $\alpha = 0$ deg it can be clearly seen that the trailing edge motion stops before the lift reaches its static value at all of the four reduced frequencies. In addition, the dynamic lift is at no time greater than the static lift because the flow is able to follow the airfoil's deflection. No stall occurs due to the trailing edge deflection at this angle of attack.

The opposite behavior appears at an angle of attack of $\alpha = 10$ deg, which is close to the stall region of the static lift curve (see figure 4a). For all reduced frequencies, an overshoot of the lift takes place, which increases with an increasing reduced frequency (see figure 7b). This behavior arises because the flow starts to separate from the airfoil's surface when the lift is increased by deflecting the trailing edge (higher flow deviation). If the trailing edge deflection is further increased, the lift decreases because the flow separation becomes larger. The overshoot only appears at angles of attack near stall because a deflection of the trailing edge just leads to a flow separation at these angles of attack. Its maximum overshoot value is approximately 3.7% of $\Delta c_{\mathrm{l,Rel}}$.

The phase shift is the delay between the trailing edge motion and the lift coefficient and is defined as

$$\phi = \frac{t^*(\Delta c_{\mathrm{l,Rel}} = 0.99) - t^*_{\beta=\max}}{t^*_{\beta=\max}} \cdot \frac{2}{\pi} \tag{10}$$

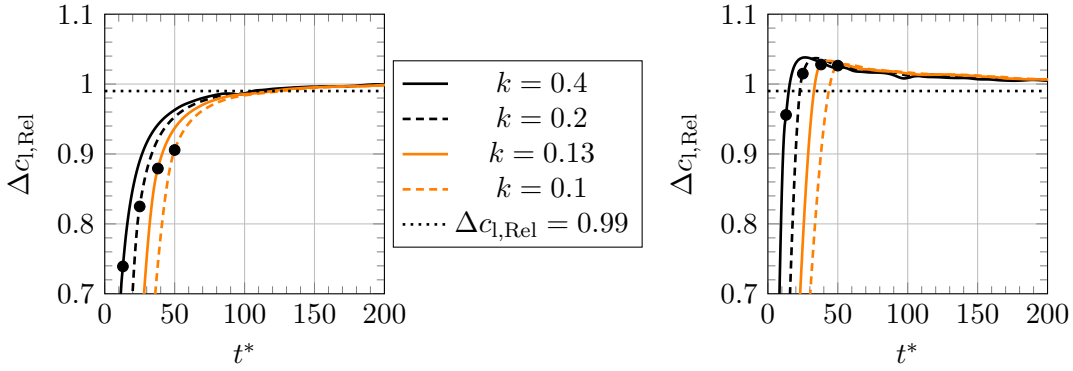

(a) $\alpha = 0$ deg (b) $\alpha = 10$ deg

Figure 7. $\Delta c_{\mathrm{l,Rel}}$ plotted against the dimensionless time t^* at four different reduced frequencies k for two different angles of attack ($\alpha = 0$ deg and $\alpha = 10$ deg) and a maximum deflection angle $\hat{\beta} = 10$ deg

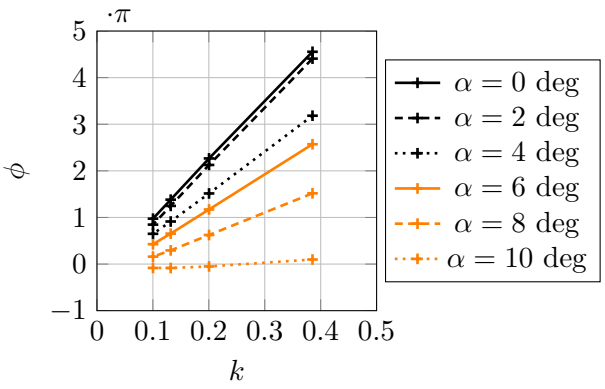

Figure 8. Phase shift ϕ plotted against the reduced frequency k for different angles of attack, $\hat{\beta} = 10$ deg

and plotted in figure 8. $t^*(\Delta c_{\mathrm{l,Rel}} = 0.99)$ describes the time when $\Delta c_{\mathrm{l,Rel}}$ passes the value 0.99 the first time and $t^*_{\beta=\max}$ describes the time when the trailing edge deflection reaches its maximum. It can be observed that the phase shift increases with increasing reduced frequency and with decreasing angle of attack. The increase due to the increased reduced frequency takes place because of the inertia of the flow. The flow cannot follow the trailing edge's motion exactly and this effect is exacerbated when the trailing edge moves faster.

The lift change caused by the trailing edge deflection is greater at lower angles of attack in comparison to higher angles of attack. If it is assumed that the duration of the trailing edge motion stays the same for different angles of attack, then the lift must change faster at lower angles of attack. The gradient of the lift depending on the deflection angle decreases with an increasing angle of attack. This can be observed in figure 8 where the phase shift decreases with increasing angle of attack.

6. Conclusions

Two-dimensional numerical investigations of a wind turbine blade's airfoil with a deformable trailing edge have been performed. These investigations included a parameter study of several deflection angles, relative chord lengths of the morphing trailing edge, and deflection shapes as well as time-resolved simulations including a dynamic trailing edge deflection with different reduced frequencies.

Actively deformed morphing trailing edges have a significant effect on the lift coefficient and the stall behavior of an airfoil. The amount of the lift change depends on the geometry (size, curvature, and deflection angle) of the deformed trailing edge. The change in lift increases with deflection angles and increasing length of the morphing trailing edge. The ratio of gained lift to aerodynamic force acting on the flap by deflecting the trailing edge shows a maximum for a morphing trailing edge between $c_{\mathrm{mte}} = 15\%$ and $c_{\mathrm{mte}} = 20\%$ with respect to the chord length of the airfoil. For larger relative chord lengths the increase of the aerodynamic force acting against the trailing edge motion is larger compared to the increase of lift. Based on this, it is assumed for the present airfoil that a length between $c_{\mathrm{mte}} = 15\%$ and $c_{\mathrm{mte}} = 20\%$ is the optimal length of the morphing trailing edge. However, this is not general and for every specific airfoil a compromise between lift gain, aerodynamic force acting on the trailing edge, and stall behavior has to be found. Furthermore, structural aspects and ease of manufacture need to be taken into account.

A phase shift between the trailing edge motion and lift coefficient was observed during the time-resolved simulations. This phase shift is positive at angles of attack between $\alpha = 0$ deg and $\alpha = 8$ deg, which means that the trailing edge motion reaches its maximum value (final deflection) before the lift coefficient. Near the stall region, the phase shift becomes negative because the deflection of the trailing edge causes flow separation followed by a decreasing lift. An overshoot of lift exceeding the static value of the lift takes place at an angle of attack of $\alpha = 10$ deg. This leads to the conclusion that the deflection of the trailing edge should only be used with caution at large angles of attack to avoid flow separation and unsteady loads caused by the flow separation.

For control strategies of deformable trailing edges, it has to be taken into account, that the phase shift between the trailing edge motion and lift coefficient increases with increasing reduced frequency and with decreasing angles of attack. Therefore, the time to reach the static lift coefficient is longer at lower angles of attack compared to higher angles of attack. In future work simulations with a control routine, which controls the deflection of the trailing edge in an unsteady flow field, should be performed in order to analyze the effect of the phase shift on the controllability of the trailing edge deflection in detail. Additionally, simulations with combined motion of the pitch and deformable trailing edge are planned. These simulations will be used to define the operating points at which the deformable trailing edge system is less effective (e.g. angles of attack near stall) so that it is more effective to use the pitch system.

Acknowledgments

The present work is funded within the framework of the joint project Smart Blades (0325601A/B/C/D) by the German Federal Ministry for Economic Affairs and Energy (BMWi) under decision of the German Federal Parliament. The authors appreciate the German Aerospace Center (DLR) for providing FLOWer. The authors thank the Leibniz Universitaet Hannover IT Services (LUIS) for the computational resources provided and Mr. A. Polaczek for his contribution to the simulation setup.

References

[1] Kaldellis J K and Zafirakis D 2011 The wind energy (r)evolution: A short review of a long history *Renewable Energy* **36** pp 1887-901

[2] Kelley N, Hand M, Larwood S and McKenna E 2002 The NREL large-scale turbine inflow and response experiment - Preliminary results *ASME Wind Energy Symp.* (Reno, Nevada) WIND2002-64 pp 412-26

[3] Barlas T K and van Kuik G A M 2007 State of the art and prospectives of smart rotor control for wind turbines *J. Phys.: Conf. Ser.* **75** 012080

[4] Pechlivanoglou G K, Wagner J, Nayeri C N and Paschereit C O 2010 Active aerodynamic control of wind turbine blades with high deflection flexible flaps *48th AIAA Aerospace Sciences Meeting* (Orlando, Florida) AIAA 2010-644

[5] Bak C, Gaunaa M, Andersen P B, Buhl T, Hansen P, Clemmensen K and Moeller R 2007 Wind tunnel test on wind turbine airfoil with adaptive trailing edge geometry *45th AIAA Aerospace Sciences Meeting and Exhibit* (Reno, Nevada) AIAA 2007-1016
[6] Ortega Gomez J, Balzani C and Reuter A 2014 Evaluation of the possibility of replacing pitch control by active trailing edge flaps in wind turbines *EWEA 2014 Annual Event* (Barcelona, Spain)
[7] Troldborg N 2005 Computational study of the Riso-B1-18 airfoil with a hinged flap providing variable trailing edge geometry *Wind Engineering* **29** (2) pp 89-113
[8] Timmer N and van Rooij R 2009 *Summary of the delft university wind turbine dedicated airfoils* Tech. rep. TU Delft
[9] Kroll N and Fassbender J K 2002 *MEGAFLOW - Numerical flow simulation for aircraft design* (Berlin: Springer)
[10] Kroll N, Radespiel R and Rossow C C 1995 Accurate and efficient flow solvers for 3D applications on structured meshes *AGARD R-807* pp 4.1-4.59
[11] Edwards J R and Chandra S 1996 Comparison of eddy viscosity-transport turbulence models for three-dimensional, shock-separated flowfields *AIAA Jour.* **34** (4) pp 756-63
[12] ASME V & V 20 Committee 2009 *Standard for verification and validation in computational fluid dynamics and heat transfer* (New York, USA: The American Society of Mechanical Engineers)
[13] Hansen M H 2007 Aeroelastic Instability Problems for Wind Turbines *Wind Energy* **10** pp 551-577